JOURNAL OF MATERIALS SCIENCE 26 (1991) 5239–5253

Exact theory of fibre fragmentation in a single-filament composite

W. A. CURTIN
BP Research, 4440 Warrensville Center Road, Cleveland, OH 44128, USA

An exact theory is developed to describe the evolution of fibre fragmentation in a single-filament composite test as a function of the underlying fibre statistical strength and fibre/matrix interfacial shear stress, τ. The fragment distribution is a complicated function of fibre strength and τ because the stress around breaks which do occur recovers to the applied value, σ, over a length $\delta(\sigma)$ determined by τ. Therefore, no other breaks can occur within $\delta(\sigma)$ of an existing break. To account for this effect, the fibre fragment distribution is decomposed into two parts; fragments formed by breaks separated by more than $\delta(\sigma)$ at stress σ, and fragments smaller than $\delta(\sigma)$ which were formed at some prior stress $\sigma' < \sigma$ when a smaller $\delta(\sigma') < \delta(\sigma)$ prevailed. The distribution of fragments larger than $\delta(\sigma)$ is identical to that of a fibre with a unique non-statistical strength σ and is known exactly. The distribution of fragments smaller than $\delta(\sigma)$ can then be determined from the distribution of the longer fragments. Predictions of the theory are compared to simulations of fibre fragmentation for several common models of stress recovery around fibre breaks with excellent agreement obtained. The present theory can be utilized to thus derive both the *in situ* fibre strength at short gauge lengths $\simeq \delta$ and the τ from experimentally obtained fragment distributions, and an unambiguous inversion procedure is briefly discussed. The application of the theory to other multiple-cracking phenomena in composites is also discussed.

1. Introduction

Composite materials composed of an epoxy resin matrix reinforced with high-strength carbon fibres are finding increasing applications due to their high specific strength and modulus. The key factors underlying the performance of these materials are the shear stress across the fibre/matrix interface and the *in situ* tensile strength of the fibres. The shear stress determines how an applied load is transferred to the strong load-bearing fibres while the fibre strength determines the ultimate load-bearing capacity of the composite. The fibre strength must be described statistically, however, because the strength is controlled by the statistical distribution of defects along the length of the fibre. The strength of a given length fibre is thus not a single value, but varies from fibre to fibre. In addition, the average fibre strength depends on the length tested: longer fibres are more likely to have more detrimental, strength-limiting defects and so are weaker, on average, than nominally identical shorter fibres. For fibre-reinforced materials, it is important to know the *in situ* strength distribution at lengths of less than 1 mm. This length fibre cannot be tested directly and hence longer (10–100 mm) weaker fibres are usually tested *ex situ*. The statistical strength at the much smaller gauge length of interest is then obtained by extrapolating from the results of tests on fibres one or two orders of magnitude larger, assuming a Weibull scaling of strength with gauge length (i.e. probability of fibre failure at stress σ and gauge length L of $P_f = 1 - \exp(-L(\sigma/\sigma_0)\rho/L_0)$ where σ_0 and L_0 are a reference length and gauge length, respectively, and ρ is the "Weibull modulus" describing the variability of strength about the mean). The reliability of such a procedure is unknown. In addition, the statistical strength of a fibre may change upon processing, and so the Weibull parameters determined *ex situ* by tensile testing may be irrelevant for describing fibre performance *in situ*. A case where such extrapolation has been shown to be erroneous has been provided by Gulino and Phoenix [1]. Taking fibres tested at gauge length 20 mm with *ex situ* mean strength of 5 GPa and Weibull modulus of $\rho = 5.6$, they measured the number of breaks versus strain *in situ*, as shown in Fig. 1a, and found that the Weibull scaling of the *ex situ* tests extrapolated to the 0.1 mm length overestimated the mean strength by up to 50%, as is evident in Fig. 1b. Fitting the data of Fig. 1a to their approximate theory, Gulino and Phoenix further estimated the Weibull moduli of the two tested fibres to be $\rho = 5.0$ and 7.8, respectively, the latter deviating significantly from the *ex situ* value of $\rho = 5.6$. Clearly, *ex situ* failure data are not always relevant to the behaviour of fibres within the composite. The fibre/matrix interfacial properties are often independently determined by pull-out experiments.

In contrast to the standard experiments, the single-filament composite (s.f.c.) test yields information on the *in situ* statistical fibre strengths at small gauge lengths and on the fibre/matrix interfacial properties simultaneously [2, 3]. The s.f.c. sample consists of a single fibre set into a dog-bone shape matrix material having a large failure strain. Subjecting the s.f.c. sample to a tensile test, a progression of breaks in the

0022–2461/91 $03.00 + .12

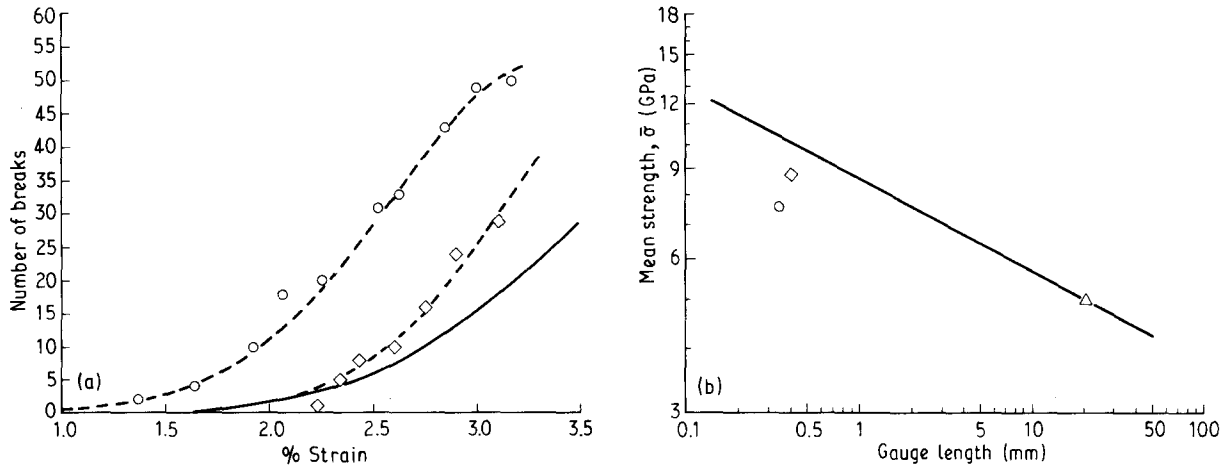

Figure 1 (a) Number of breaks versus strain measured in s.f.c. tests on two fibres. (——) Predicted behaviour using *ex situ* strength data on 20 mm fibres (mean strength $\bar{\sigma} = 5.6$ GPa, Weibull modulus $\rho = 5.6$). (– – –) Fits to theory of Gulino and Phoenix (1), fitting parameters (○) $\bar{\sigma} = 7.6$ GPa, $\rho = 5.0$ and (◇) $\bar{\sigma} = 8.8$ GPa, $\rho = 7.8$. (b) Mean strength versus gauge length. (——) Extrapolation of *ex situ* data at 20 mm; (○, ◇) $\bar{\sigma}$ from fits to (1a). Note the overestimate of $\bar{\sigma}$ at small gauge lengths obtained by extrapolation.

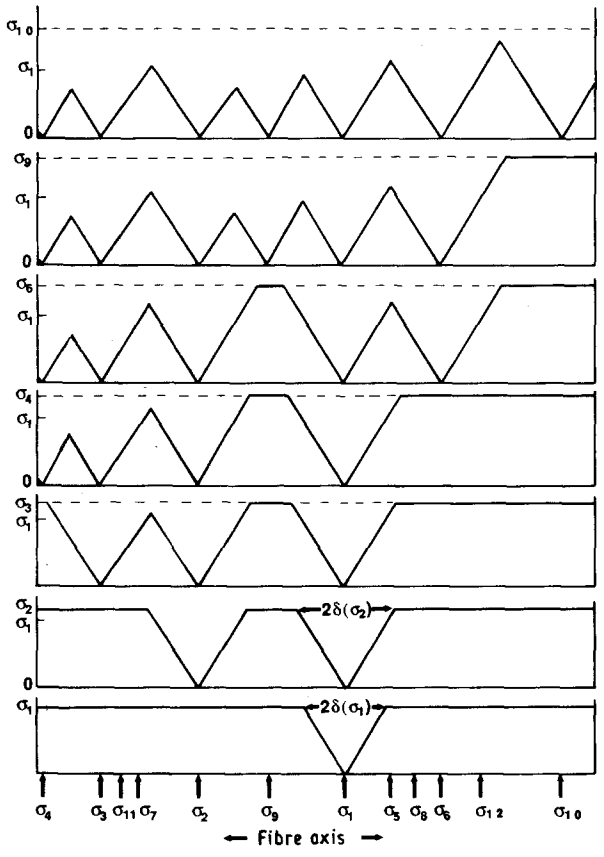

Figure 2 Schematic illustration of a single-filament composite test. The stress profiles along the fibre axis as a function of applied stress are shown. The weakest 12 defects at strengths $\sigma_n = n^{1/5}\sigma_1$, randomly located along the fibre are marked explicitly. Breaks occur at these defect sites and the stress recovers linearly from zero at the break to the applied stress, σ, over length $\delta(\sigma)$. If defect n is closer than $\delta(\sigma_n)$ to a weaker defect $n' < n$, defect n falls within the stress recovery region of the break at n' and never breaks, as for $n = 5, 7, 8, 11, 12 \rightarrow \infty$. The fragment lengths are the distances between breaks; increasing stress creates more and shorter fragments.

fibre are observed (see Fig. 2). The fibre sustains multiple breaks because the matrix holds the composite together. With increasing tensile stress, the first break occurs at the weakest point along the fibre. The tensile stress in the fibre recovers from zero at the fibre break to the applied value over a length of δ which depends on both the applied stress and the shear stress, τ, transferred across the fibre/matrix interface. Increasing the stress further increases the length δ and also introduces additional breaks at weak points along the fibre. Because the stress within a recovery length δ is always below the applied stress, as we will show below, subsequent nearby breaks are always separated by at least a distance δ.

Eventually, at a sufficiently large stress, the fragmentation process ceases because each point along the fibre is within the recovery length of some break and therefore no more breaks can occur. The raw data from the s.f.c. test thus consist of a record of the location of each break and the stress at which that failure occurred. The data are usually reformulated, at various stress or strain increments, into a fibre fragment distribution, where a fragment is the region of intact fibre between two neighbouring breaks. Another simpler reformulation of the data is into a record of how many total breaks have occurred as a function of stress or strain as in Fig. 1a. It is clear from this description of the s.f.c. test that the data contain a wealth of information on the *in situ* fibre strength at small gauge lengths (of order δ) and on the interfacial shear strength, τ. However, because the recovery length, δ, changes with stress and because new breaks cannot occur close to prior breaks, the effects of the underlying fibre strength and interfacial shear strength are not easily separated. The problem to date has thus been one of extracting these quantities out of the s.f.c. test data, because no complete theory of the fragmentation process exists when the fibre strength is statistically distributed.

For unique strength fibres, the fragment distribution can be derived exactly, however [4]. By "unique strength fibre" we mean that the strength distribution is approaching a delta function (the "Weibull modulus" is nearly infinite) and hence the strengths of the weakest and strongest defects become identical. Nonetheless, the defects can still be ordered from weakest to strongest so that the breaks will occur in a well defined order. In this case, all the data in the s.f.c. test are generated at the unique strength, σ_0, and there is a unique recovery length, $\delta_0 \equiv \delta(\sigma_0)$ that does

not change during the test. Thus, at the end of the s.f.c. test all the fibre fragments must be between the lengths δ_0 and $2\delta_0$. The upper limit of $2\delta_0$ arises because if a fragment of length greater than $2\delta_0$ exists, the region near the centre still feels the applied stress and will break, leading ultimately to at least two smaller fragments between lengths δ_0 and $2\delta_0$ [5]. The length $2\delta_0$ is precisely the "critical length", l_c, discussed by Kelly and Tyson. The fragment distribution at completion is not uniform between δ_0 and $2\delta_0$, however, and the mean fragment length $\bar{x}$ is $\bar{x}/\delta_0 = 1.337$ (see also [6]). So, if the fibre strength is uniform then the desired mean stength, σ_0, and recovery length, δ_0, could be obtained directly. Under the further assumption that the matrix is perfectly plastic with a shear strength τ, the value of τ can then be obtained from the relation

$$\tau = \frac{\sigma_0 d}{4\delta_0} = \frac{\sigma_0 d}{2l_c} \quad (1)$$

where d is the fibre diameter. However, the true $\delta(\sigma)$ relationship cannot be determined from the experiment. In addition, the evolution of the fragment distribution with fragment number does not provide any additional information in this case.

When the fibre strength distribution is not unique (i.e. for real fibres), the interpretation of the s.f.c. test is much more difficult. The distribution in strengths implies a changing recovery length $\delta(\sigma)$ as the test proceeds. At completion of the test at stress σ_{max}, there is still a maximum possible fragment length $2\delta(\sigma_{max})$. However, the minimum fragment length is always smaller than $\delta(\sigma_{max})$ because earlier in the test, at stress $\sigma < \sigma_{max}$, there is some chance that two breaks can occur as close as $\delta(\sigma) < \delta(\sigma_{max})$. Henstenburg and Phoenix [3] have performed Monte Carlo simulations of the fragmentation process for particular $\delta(\sigma)$ relations and have formulated an empirical relation between the final mean fragment length and the Weibull modulus governing the fibre strength distribution. Fraser *et al.* [7] have also performed simulation studies of the fragmentation process and Drzal et al. [8, 9] and Own *et al.* [10] have attempted to account for the statistical aspects of this problem by fitting fragment distributions to Weibull and log normal forms. However, no progress has been made in predicting the fragment distributions analytically, despite the fact that the full evolution of the fragment distribution with increasing stress provides all the information needed to deconvolute the strength distribution and the $\delta(\sigma)$ relationship from experimental data.

In this paper, we develop an exact theory of the full evolution of the fragment distribution. The crux of the theory is based on viewing the fibre fragments in two parts: (i) those fragments formed by breaks separated by more than $\delta(\sigma)$ at the current stress level σ, and (ii) those fragments smaller than δ which were formed at an earlier stress level $\sigma' < \sigma$ when a shorter $\delta(\sigma') < \delta(\sigma)$ prevailed. The distribution of fragment lengths in part (i) (all fragments larger than $\delta(\sigma)$) is the same as that for a fibre with a unique strength, σ, and is known exactly. The distribution of lengths in part (ii) (all fragments shorter than $\delta(\sigma)$) can be monitored exactly using certain aspects of the distribution of lengths in part (i). We subsequently use this theory to predict the fragment distribution for tests on fibers with distributed strengths and our results compare very well with the computer simulation results of Henstenburg and Phoenix [3] for a range of $\delta(\sigma)$ relations. The remainder of this paper is organized as follows. In Section 2 we analyse the fibre fragmentation process and show it can be formulated as a set of differential equations involving only the fragment distribution of a unique-strength fibre, which is known. In Section 3, the theory of Section 2 is shown to predict fragment distributions for varying fibre Weibull moduli and stress-recovery rules which are in excellent agreement with the simulation studies of Henstenberg and Phoenix. In Section 4 we discuss other applications of the same theory and summarize our main findings. Appendix 1 discusses some subtleties which can arise in properly defining the exclusion length $\delta(\sigma)$ in the presence of elastic shear stresses. Appendix 2 discusses other restrictions on the form of a spatially dependent shear stress, $\tau(x)$, for proper application of the theory. Appendix 3 contains a discussion of the uniform-strength fragment distribution and Appendix 4 discusses some mathematical and computational aspects of this problem.

2. Theory of fragment distribution

Before proceeding, it is useful to discuss first the nature of the stress recovery length, δ, and, moreover, the role δ plays in precluding the occurence of close fibre failure locations (i.e. small fragments). At a fibre break, the axial tensile stress in the fibre is precisely zero and the matrix carries the load. As one moves away from the break position along the fibre, however, the axial stress in the fibre begins to increase due to stress transferred from the matrix through the interface. Mechanical equilibrium considerations show that the average axial stress $\sigma(x)$ at a distance x from the break is related to the (possibly spatially varying) shear stress $\tau(x)$ at the interface by the relation

$$\sigma(x) = \frac{4}{d}\int_0^x \tau(x')\,dx' \quad (2)$$

where d is the fibre diameter (see [11] for further discussions). The recovery length, δ, is the distance at which $\sigma(x)$ has reached the "applied" fibre axial stress, σ_{app}*

$$\sigma(\delta) = \frac{4}{d}\int_0^\delta \tau(x')\,dx' = \sigma_{app}, \quad (3)$$

and so δ depends on the form of $\tau(x)$ and on σ_{app}. In our discussion here, we take $\tau(x)$ to be independent of

* One problem we have not addressed here is how to determine the applied axial fibre stress. The composite strain and fibre strain are often not the same, making identification of the actual fibre stress a potential difficulty in practice. The present theory assumes this "applied" fibre stress is known during the test.

σ_{app} and δ; we address these issues further in Appendices 1 and 2. Then, the stress $\sigma(x)$ within the recovery length $x < \delta$ is independent of σ_{app}; it is only the length of recovery δ which changes with σ_{app}. Furthermore, because $\tau(x)$ is non-negative, the stress within the recovery region $x < \delta$ is always less than σ_{app}

$$\sigma(x) < \sigma_{app} \qquad x < \delta \tag{4}$$

and does not changes as σ_{app}, and hence δ, is increased.

The consequences of this are as follows, and are schematically shown in Fig. 2 assuming for demonstration purposes that τ is a constant. First, if a break at $x = 0$ occurs at stress σ^*, then the stress in the recovery region $x < \delta^*$ is forevermore below σ^*. Because no points along $x < \delta^*$ failed at the prior applied stresses $\sigma < \sigma^*$, no failures can occur in $x < \delta^*$ at any future applied stress. For even if $\sigma > \sigma^*$, the stresses in $x < \delta^*$ remain below σ^* and no failure can occur. Second, consider a point $x > \delta^*$. As the applied stress increases, the stress at x increases and δ increases beyond δ^*. If $\delta = x$ is reached at a stress lower than the failure stress of point x, with no intervening failures, then the point x enters the stress recovery region of the break at $x = 0$ and can never attain the stress required to fail (as is the case for the point at σ_5 in Fig. 2, which falls within the recovery region of point σ_1 at a stress below σ_5). Thus, any region of unbroken fibre within the stress recovery length of some break cannot fail. Failures only occur at points which have not yet been subsumed by the stress recovery length δ around the existing breaks. The stress-dependent recovery length, δ, thus creates an exclusion region about each fibre break which precludes the occurrence of any further fibre failures. This conclusion is independent of the detailed nature of $\tau(x)$ (see Appendices 1 and 2, however).

Overlapping of stress-recovery regions can occur if the failure stress of point x, σ^x, is attained before $\delta = x$. Then, the point x fails and forms a stress recovery region or exclusion zone of length $\delta(\sigma^x)$. The stress recovery regions around x and 0 may overlap at σ^x, i.e. $x < 2\delta(\sigma^x)$, to form a fibre fragment which will remain unaltered for the remainder of the s.f.c. test (in Fig. 2, the fragment between points σ_2 and σ_3 formed at σ_3, for example). Or, the stress recovery regions may overlap at some higher stress $\sigma > \sigma^x$ satisfying $x = 2\delta(\sigma)$ if no intervening failures occur (no case shown in Fig. 2). Or, finally, additional failures between points 0 and x may occur at higher stresses, leading to additional fibre fragments (as shown in Fig. 2 by the break at point σ_9 which occurs between σ_1 and σ_2). In any case, it is important to note that once any two stress recovery regions (exclusion zones) do overlap, the resulting fragment remains unchanged for the remainder of the s.f.c. test.

With the above understanding of the role of δ as an exclusion zone, we can now describe a procedure to calculate the fragment distribution as a function of stress. Imagine the s.f.c. test on a fibre of length L_T to have proceeded up to stress σ, with a corresponding recovery length $\delta(\sigma)$ at this point in the test, and that there are a total of N_T fragments ($N_T - 1$ breaks). Now remove from consideration the N_R fragments of length $x < \delta(\sigma)$ which occupy a combined length L_R of the fibre and store them in a distribution $P_R(x)$ (the subscript R reminds us that this is the distribution of the removed fragments). *Because these fragments are shorter than $2\delta(\sigma)$ they will remain unchanged during the rest of the s.f.c. test.* The remaining $N_T - N_R - 1$ breaks are distributed along an effective fibre length $L_T - L_R$. Each break has a recovery length $\delta(\sigma)$ around it and by construction, no two breaks are closer than $\delta(\sigma)$. *Therefore, the fibre fragment distribution for this remaining portion of fibre, of length $L_T - L_R$, is identical to the fragment distribution of a fibre of unique strength σ, length $L_T - L_R$, and number of breaks $N_T - N_R$,* corresponding to a dimensionless break density

$$\frac{N_T - N_R}{L_T - L_R}\delta = n\delta \tag{5}$$

Let $P(x; n, \delta)$ denote this unique strength distribution. $P(x; n, \delta)\,\Delta x$ is the fraction of fragments of length between x, $x + \Delta x$ at recovery length δ and break density $n\delta$ and is known exactly, as discussed in Appendix 3. The fragment distribution of the entire fibre at this stress is the sum of the removed distribution $P_R(x)$, which describes all the fragments of length $x < \delta$, and $P(x; n, \delta)$, which describes all the fragments of length $x > \delta$.

At this point, we have just conceptually divided the fragment distribution into two parts, $P_R(x)$ for $x < \delta$ and $P(x; n, \delta)$ for $x > \delta$. We know the unique-strength distribution $P(x; n, \delta)$ so what is required is $P_R(x)$ and the fragment density, n, in the remaining portion of the fibre at each stress level during the test. We thus examine how the distribution $P_R(x)$ for $x < \delta$ and density $n = N_T - N_R/L_T - L_R$, evolve with increasing stress. To do so, we next increase the applied stress by a small increment, $\Delta\sigma$, and hence increase the recovery length by $\Delta\delta$, and analyse the changes to $P_R(x)$ and n. Now those fragments previously removed from consideration at stress σ remain unchanged at stress $\sigma + \Delta\sigma$, of course. But, at the new length $\delta + \Delta\delta$, those fragments between δ and $\delta + \Delta\delta$ in length are now smaller than $\delta + \Delta\delta$ and must also be removed from consideration. The fraction of fragments in this length range is $P(x = \delta; n, \delta)\Delta\delta$ and so the total number of such fragments is

$$\Delta N_R = (N_T - N_R)P(\delta; n, \delta)\Delta\delta \tag{6}$$

and their total length is

$$\Delta L_R = \Delta N_R \delta. \tag{7}$$

The above ΔN_R fragments, all of length between δ and $\delta + \Delta\delta$, must be added to the removed distribution $P_R(x)$. The change in $P_R(x)$ is thus

$$\begin{aligned} \Delta P_R(x) &= \Delta N_R \qquad \delta < x < \delta + \Delta\delta \\ &= 0 \qquad \text{all other } x \end{aligned} \tag{8}$$

These ΔN_R fragments are the only contribution to $P_R(x)$ at lengths $\delta < x < \delta + \Delta\delta$. From Equations 6 and 8 we see that the evolution of $P_R(x)$ is determined solely by the known function $P(\delta; n, \delta)$ evaluated at length δ and density n.

Returning to the remaining, unremoved, portion of the fibre, we now follow the evolution of the break density n. The length of this portion of fibre at stress $\sigma + \Delta\sigma$ is now $L_T - L_R - \Delta L_R$ because the length ΔL_R has also been removed. The number of breaks in this portion of fibre is $N_T - N_R$ minus ΔN_R but also plus the number ΔN_A of new breakable defects encountered between stresses σ and $\sigma + \Delta\sigma$. To determine ΔN_A, we note that because only regions of fibre a distance δ or more away from a break can fail, and because each fragment is bounded by a break on each side, only fragments of length $x > 2\delta(\sigma)$ can incorporate another break. And, such a break can only occur in the available length x-2δ. Therefore, the number of breaks ΔN_A added to the remaining fibre is

$$\Delta N_A = \mu(\sigma, L^*)\Delta\sigma \tag{9}$$

where $\mu(\sigma, L)\,\Delta\sigma$ is the number of defects of strength between σ and $\sigma + \Delta\sigma$ in a length L of fibre, and L^* is the total length of remaining fibre able to incorporate a break

$$L^* = (N_T - N_R - \Delta N_R)\int_{2\delta}^{\infty} dx(x - 2\delta)\,P(x; n, \delta). \tag{10}$$

The function $-\mu(\sigma, L)$ characterizes the statistical strength of the fibre and is often approximated as a Weibull distribution. In total, at stress $\sigma + \Delta\sigma$, the remaining fibre length is

$$L = L_T - L_R - \Delta L_R, \tag{11a}$$

the remaining number of breaks, N, is

$$N = N_T - N_R - \Delta N_R + \Delta N_A \tag{11b}$$

and the break density is simply

$$n = N/L \tag{12}$$

The fragment distribution for lengths $x > \delta + \Delta\delta$ is then simply given by $P(x; n, \delta + \Delta\delta)$. The evolution of the total fragment distribution is thus completely and exactly described by the physical parameters ultimately to be derived from experiment, i.e. the $\delta(\sigma)$ relation and the fibre strength distribution $\mu(\sigma, L)$, and which serve as input into the theory, and by the unique-strength fragment distribution $P(x; n, \delta)$ which is known exactly.

The process discussed conceptually above in Equations 6–12 is more clearly and concisely described by a set of differential equations for the evolution of the length L and number of breaks N in the remaining fibre and of the removed distribution (unnormalized) P_R which follow from the above by taking $\Delta\sigma \to d\sigma$ and $\Delta\delta \to d\delta$

$$\frac{dL}{d\sigma} = -N\delta P(\delta; n, \delta)\frac{d\delta}{d\sigma} \tag{13a}$$

$$\frac{dN}{d\sigma} = -NP(\delta; n, \delta)\frac{d\delta}{d\sigma} + \mu(\sigma, L^*) \tag{13b}$$

$$L^* = N\int_{2\delta}^{\infty} dx(x - 2\delta)\,P(x; n, \delta) \tag{13c}$$

$$n = N/L \tag{14}$$

and

$$\frac{dP_R(x)}{d\sigma} = NP(\delta; n, \delta)\frac{d\delta}{d\sigma}\delta_D(x - \delta) \tag{15}$$

where $\delta_D(\,)$ in the final equation denotes the Dirac delta-function. The initial conditions for Equations 13 and 15 are $L(\sigma = 0) = L_T$, $N(\sigma = 0) = 0$ and $P_R(x; \sigma = 0) = 0$. These equations are easily solved up to applied stress, σ_{app}, to yield the two parts $P_R(x)$, $x < \delta$ and $P(x; n, \delta)$, $x > \delta$ of the full fragment distribution. These simple equations are the main result of the present work.

Some qualitative features of the evolution of the fragment distribution are as follows. At low numbers of breaks (low stresses) the dimensionless break density, $n\delta$, is low and the probability of removing any breaks is roughly proportional to $(n\delta)^2$, which is negligible. The total fragment distribution is then very nearly $P(x; n, \delta)$. Likewise, for nearly unique strength, the number removed at any density is vanishingly small and again the total distribution is $P(x; n, \delta)$. At higher stresses and broader strength distributions the "removed" distribution, $P_R(x)$, can, however, represent a large fraction of the total distribution; below we show that at completion of the test a fibre of Weibull modulus $\rho = 3$ has about 65% of its fragment distribution in P_R while for $\rho = 5$ [10], about 59% (50%) of the distribution is in P_R. Hence, this contribution is crucial in order accurate to follow the evolution of the fragment distribution over a wide range of ρ values.

To reiterate, our formulation of the fragment distribution of distribution strength fibres is seen to reduce the entire problem to one of knowing only the unique-strength distribution $P(x; n, \delta)$, which has a tractable exact solution (see Appendix 1). Thus, given an experimental set of fragment distributions at known stresses, the desired fibre statistics $\mu(\sigma, L)$ and interfacial quantities contained in the $\delta(\sigma)$ relation can, in principle, be obtained by appropriate inversion procedures.

3. Fragment distributions: Weibull fibre strength

In this section we solve Equations 13–15 using results given in Appendix 3 for $P(x; n, \delta)$ and demonstrate the quantitative success of the theory. We specialize to the case where the fibre strength is of the Weibull form, which is usually assumed to hold for real composite systems, but the theory is by no means restricted to this special case. Also, our predictions for the fragment distribution can then be compared directly to the simulation results of Henstenburg and Phoenix [3].

The Weibull form for the fibre strength distribution for a fibre of length L is

$$\mu(\sigma, L) = \frac{L}{L_0}\frac{\rho}{\sigma_0}(\sigma/\sigma_0)^{\rho-1} \tag{16}$$

where L_0 is the fibre gauge length appropriate to the scale parameter σ_0 and ρ is the Weibull modulus [3]. Note that this form for $\mu(\sigma, L)$ assumes that defects in the fibre are spatially uncorrelated and thus that the

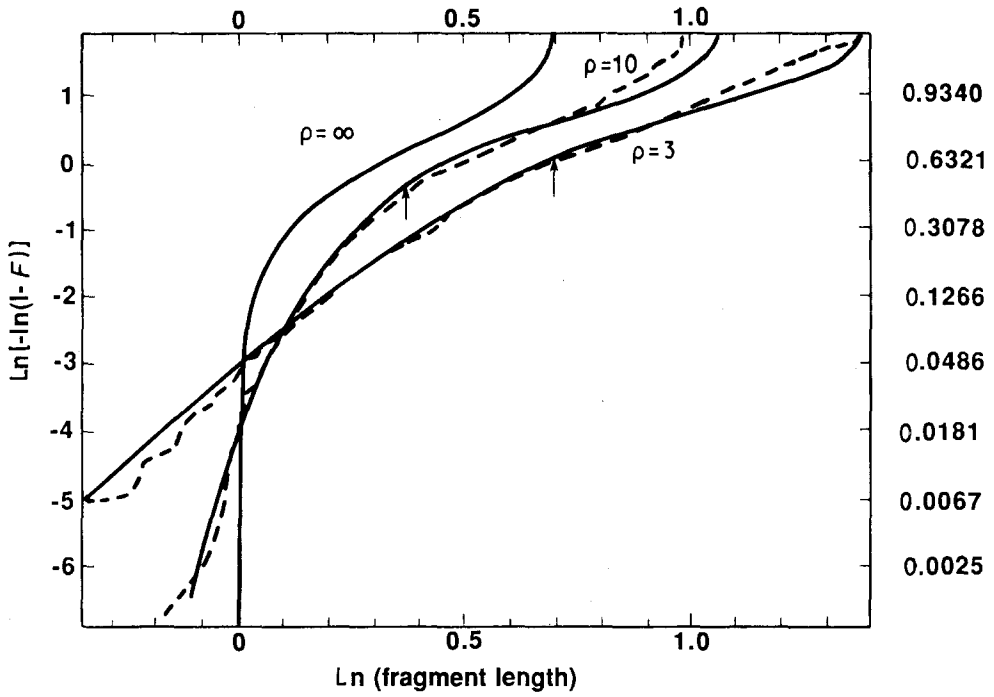

Figure 3 Weibull plots of the (——) predicted and (– – –) simulated final fragment distributions for linear stress recovery; $\ln[-\ln(1-F)]$, with F the cumulant of the fragment distribution, versus ln (fragment length) for several values of Weibull modulus, ρ, at fibre length $L_T/\delta_R = 200$. The fragment length is normalized to the reference length δ_R (see text). Arrows denote longest fragment lengths contained in the "removed" distribution P_R, which constitute a substantial fraction of the total distribution at moderate ρ.

probability of finding any type of defect scales linearly with fibre length. Insight into the scale parameters L_0 and σ_0 is gained by recognizing that σ_0 is the applied stress required to cause exactly (on average) one failure in a fiber of length L_0.

3.1. Linear stress recovery

Here we further specialize to the situation where the shear stress is assumed constant, $\tau(x) = \tau$, so that the recovery length is linear with stress, $\delta = d\sigma/4\tau$. It is convenient to introduce reference length and stress scale parameters to put all quantities in nondimensional form. As discussed in Appendix 4, the reference stress scale is chosen to be the fibre strength, σ_R, at the reference gauge length, $2\delta_R$ (with $\delta_R = d\sigma_R/4\tau$), which yields

$$\sigma_R = \left(\frac{2\tau}{d} L_0 \sigma_0^\rho\right)^{1/(\rho+1)} \tag{17}$$

and is the same as that selected by Henstenburg and Phoenix [3].

Predictions for the final fibre fragment distribution for a range of ρ are shown in Fig. 3. The ρ values, and the fixed value of $L_T = 200$, correspond precisely to cases studied by Henstenburg and Phoenix, and their results are also shown in Fig. 3. The predicted distributions agree very well with the simulation results at all ρ. There are some deviations at the largest fragment lengths and for intermediate values of ρ, $\rho \simeq 10$, but we suspect the theory lies within the error bars (not given in [3]) of the simulations, because at each ρ the simulation data are the average of only five realizations. Also, the variations in the simulation values of the final stress for $\rho = 5$ vary by $\pm 10\%$ from the mean value, for ten realizations, suggesting wide fluctuations at least near the end of the test. The predicted and simulated number of fragments N_T at the end of the test are shown in Table I and agree well for all ρ, noting that for the ten realizations at $\rho = 5$, N_T varied between 109 and 119. The mean fragment length is shown in Fig. 4, and our results are within the error bars of the simulation results, the deviations being largest again in the intermediate range of Weibull modulus values, $10 \leq \rho \leq 20$. Also shown in Fig. 3 are the points at which the distribution $P_R(x)$ ends and $P(x; n, \delta)$ begins; as noted earlier a considerable portion of the fragment distribution resides in $P_R(x)$. These results clearly show that the unique-strength distribution ($\rho = \infty$) is very inadequate for describing fragment distributions of real fibres, for which $\rho \leq 15$ is typical.

TABLE I Theory and simulation [3] results for mean number of fragments versus Weibull modulus, ρ, for linear recovery (nominal fibre length $L_T = 200$)

ρ	L_T	N_T(sim)	N_T(theory)
3	198.4	103	102.8
5	198.5	113	111.5
10	199.1	124	123.7
15	199.1	129	129.7
∞		149	149
(1000)			

The above comparison was confined to only the details of the final fragment distribution. The theory also predicts the full evolution toward that final distribution, and sample results for $\rho = 5$ are shown in Fig. 5; experimental/simulation results are not available for comparison, unfortunately. Another manifestation of the accuracy of our approach to the

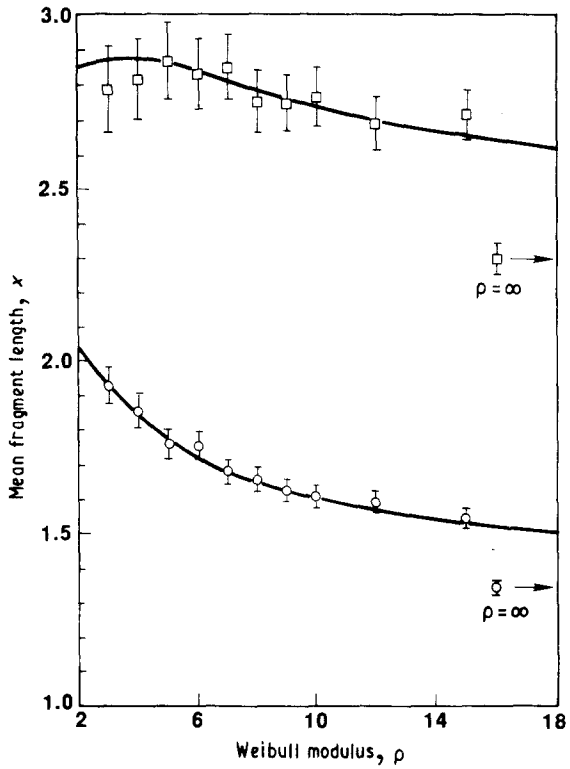

Figure 4 Mean fragment lengths $\bar{x}/\delta_R$ as (——) predicted and obtained by simulation versus Weibull modulus, ρ, for (○) linear recovery and (□) bilinear recovery ($\sigma_b/\sigma_R = 0.7$, $\tau_f/\tau = 0.3$). $L_T/\delta_R = 200$.

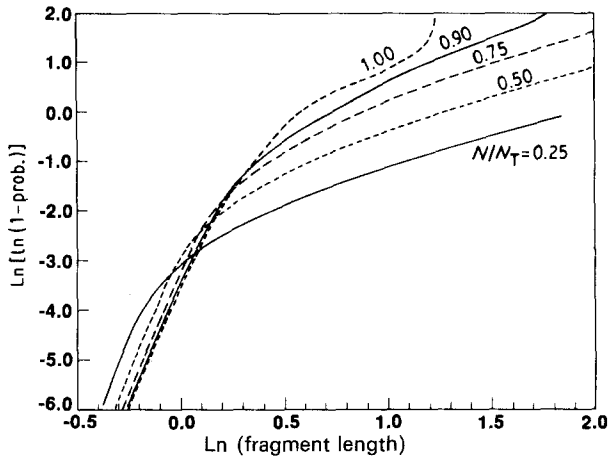

Figure 5 Weibull plot of predicted evolution of the fragment distributions with increasing stress, shown at various break fractions, for linear recovery and ρ = 5, $L_T/\delta_R = 200$.

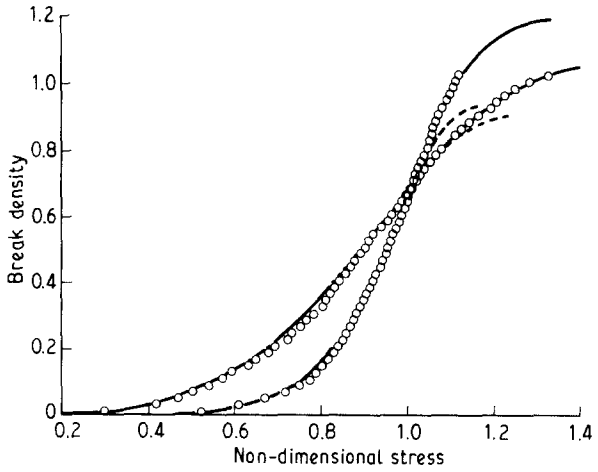

Figure 6 Dimensionless break density $N L_T/\delta_R$ versus stress for ρ = 4, 8 as predicted by (——) the present theory, (– – –) the theory of Gulino and Phoenix [1], and (○) by simulation.

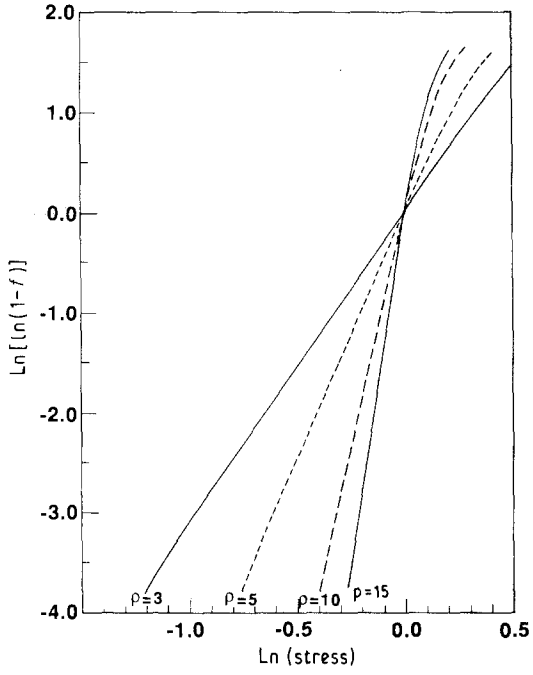

Figure 7 Weibull plot of number of breaks versus stress for linear recovery and a range of ρ values. The data are nearly linear up to at least $f = 0.75$, with slopes close to the actual ρ values.

evolution of the distribution is in a comparison between theory and simulation of the number of breaks as a function of stress. The dimensionless break density $2N\delta_R/L_T$ versus dimensionless stress σ/σ_R, is shown in Fig. 6 for two values ρ = 4 and ρ = 8. Agreement with the simulation data is again excellent over the entire stress range covered by the s.f.c. test. Also shown in Fig. 6 are the results of a simple theory of Gulino and Phoenix [1]. This theory is accurate at lower densities and has a simple analytical form, but fails at higher densities in a ρ-dependent manner. Considering the cumulative probability of finding a break as a function of stress normalizes the number of breaks, N, in the experiment and the theory by the total number N_T. Obtaining the cumulative probability after N breaks as $f = (N - 0.5)/N_T$, as done by Henstenburg and Phoenix [3], we find that (see Fig. 7) a Weibull plot of $\ln(-\ln(1-f))$ versus $\ln(\sigma/\sigma_R)$ yields very nearly a straight line, and these predicted results are essentially in perfect agreement with the simulation results. Why the distribution of breaking stresses follows a Weibull form over such a wide range of stress (it should be Weibull at low stresses, of course) is not understood. But, the fact that the apparent Weibull modulus, $\hat{\rho}$, is close to the actual ρ should be of considerable value in devising a means to obtain ρ, σ_R, δ_R and $\delta(\sigma)$ from experimental data.

3.2. Bilinear stress recovery

Henstenburg and Phoenix [3] have also considered the next level of complication in the $\delta(\sigma)$ relation by

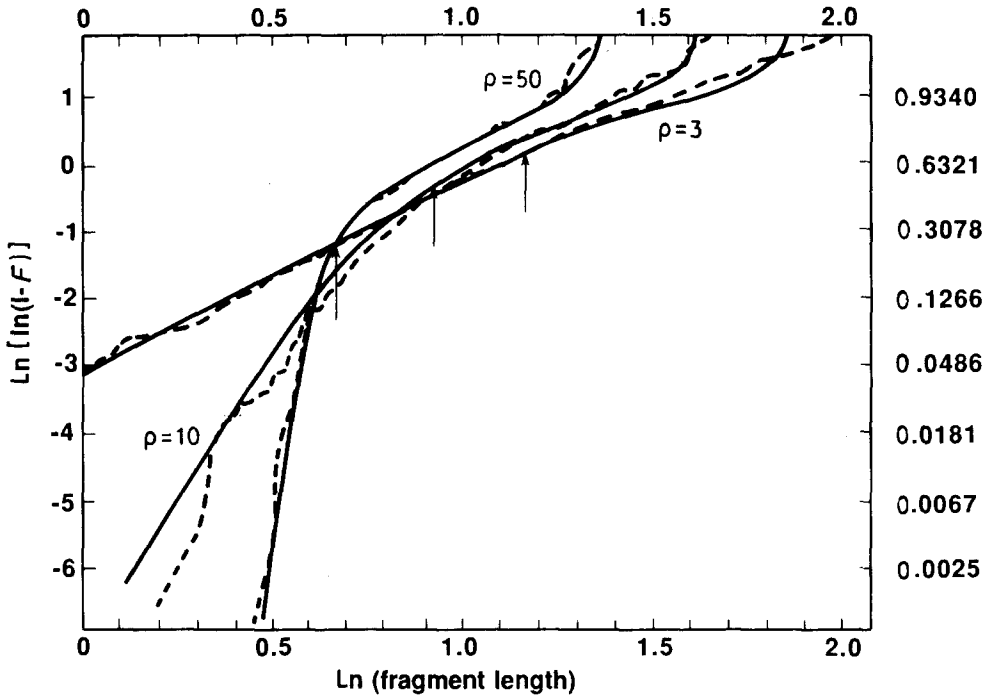

Figure 8 As Fig. 3 but for bilinear recovery ($\tau_f/\tau = 0.3$, $\sigma_b/\sigma_R = 0.7$) for $\rho = 3$, 10, 50.

allowing debonding starting at the fibre break with a frictional shear stress along the length of the debond. It is assumed that the usual linear stress recovery, $\delta = d\sigma/4\tau$, with τ perhaps interpreted as a yield stress, holds up to a critical length, δ_b, and that for larger stresses a debonded region forms behind the yield region with constant frictional stress, τ_f. For stresses $\sigma > \sigma_b$ such that $\delta > \delta_b$, the stress recovery length is then determined by

$$\sigma = \sigma_b + \frac{4}{d}\int_0^{\delta - \delta_b} dx\, \tau_f \qquad (17)$$

where $\delta - \delta_b$ is the debonded length. Solving for δ yields

$$\delta = \sigma_b + \frac{d}{4\tau_f}(\sigma - \sigma_b) \qquad \sigma \geq \sigma_b \qquad (18)$$

This modification introduces two additional parameters, σ_b and the ratio τ_f/τ, into the problem. We may still continue to use the scale factors σ_R and δ_R to non-dimensionalize the problem, however, and so input to any calculation consists of ρ, σ_b/σ_R, τ_f/τ and L_T.

In Fig. 8 we show our predicted final fragment distributions for various ρ values for the fixed values of $\sigma_b/\sigma_R = 0.7$, $\tau_f/\tau = 0.3$ and $L_T = 200$. As previously, these results compared well with the simulation data. The final mean fragment lengths, shown in Fig. 4, and the total number of breaks as exhibited in Tables II and III are also in agreement for a range of σ_b/σ_R and τ_f/τ values. The cumulative number of breaks versus stress plotted in Weibull form is shown in Fig. 9 for $\rho = 5$, $\tau_f/\tau = 0.3$ and a range of σ_b/σ_R. The dependence is again nearly Weibull-like but there is systematic curvature to some of the results in Fig. 9. The apparent Weibull modulus $\hat{\rho}(\rho)$ is slightly different from that obtained using the linear stress recovery model but is not very sensitive to the value of σ_b/σ_R.

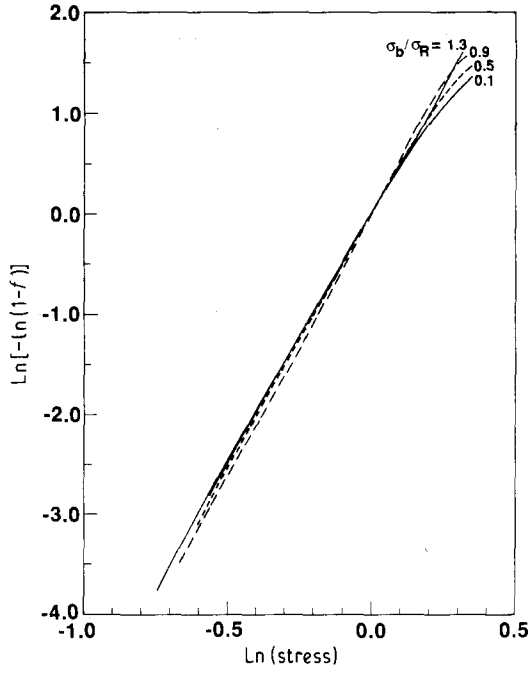

Figure 9 Weibull plot of fraction of breaks versus normalized stress for $\rho = 5$, bilinear recovery, $\tau_f/\tau = 0.3$ and various σ_b/σ_R; note the insensitivity to σ_b/σ_R.

Comparing the linear stress recovery to the bilinear stress recovery distributions, overall the same qualitative dependence on ρ is obtained and the quantitative differences reside mainly in differences in mean properties such as $\bar{x}/\delta_R$. Because the underlying δ_R are unknown in a real experiment, our results suggest that inverting experimental data to determine $\delta(\sigma)$ is a subtle task.

3.3. Summary

The theory of Section 2 has been shown to agree well with all aspects of the available computer experiments.

The full power of the theory is that, as opposed to the arduous task of performing many simulations, the fragment distributions for any σ_0, L_0, ρ, L_T and $\delta(\sigma)$ relation are essentially trivial to calculate with high accuracy. Therefore, the inverse problem of determining the σ_0, L_0, (or σ_R and δ_R) ρ and $\delta(\sigma)$ from a given set of experimental data is, in principle, now far more easily and efficiently accomplished than previously. In the next section, we discuss some details of such a procedure and examine the sensitivity of the fragment distribution to the $\delta(\sigma)$ relation.

4. Discussion

With the ability to predict accurately all the details of the fragmentation process given ρ, τ, σ_0, L_0, τ_f/τ and σ_b, we now briefly investigate the prospects for inverting experimental data to derive these quantities. As noted at the close of the previous section, a Weibull plot of the cumulative number of breaks f versus stress yields a good straight line of slope $\hat{\rho}$, which is close to the true Weibull modulus ρ. On the other hand, this behaviour is not all that sensitive to the detailed $\delta(\sigma)$ relation. To highlight this, Fig. 10 shows f versus stress for a particularly bilinear recovery ($\rho = 5$, $\tau_f/\tau = 0.3$ and $\sigma_b/\sigma_R = 0.7$) as well as for several linear recovery cases ($\tau_f/\tau = 1.0$, $\sigma_b/\sigma_R = 0.0$, for various values of ρ near $\rho = 5$). Evidently, because these plots are quite similar, the number of breaks f versus stress is rather robust for obtaining approximate ρ values but is, therefore, not useful for obtaining $\delta(\sigma)$ data. At least one additional distribution is needed to aid in interpreting the data. Here, we will select the final fragment length distribution, which appears to depend more sensitively on the $\delta(\sigma)$ relation, as the second distribution to fit. To see that f versus stress and the final fragment distribution are in some ways complementary, consider again Fig. 10.

TABLE II As Table I, but for bilinear recovery $\sigma_b/\sigma_R = 0.7$, $\tau_f/\tau = 0.3$

ρ	L_T	N_T(sim)	N_T(theory)
3	197.7	71	69.1
5	197.3	69	69.3
10	199.1	72	72.7
15	198.0	73	74.6
∞	198.8	87	86.6

One might erroneously conclude that the f versus stress for ($\rho = 5$, $\tau_f/\tau = 0.3$, $\sigma_b/\sigma_R = 0.7$) was due to a linear recovery model with $\rho \simeq 5.50$. However, comparing the final fragment distribution for ($\rho = 5$, $\tau_f/\tau = 0.3$, $\sigma_b/\sigma_R = 0.7$) to that for linear recovery at various ρ, as shown in Fig. 11, we find that the best fit linear recovery model corresponds to a ρ between 2 and 3. Thus, the linear recovery model with a single ρ value cannot accurately fit both the number of fragments with stress and the final fragment distribution obtained from the bilinear recovery distributions. This indicates that with these two distributions we have some sensitivity in determining ρ and the $\delta(\sigma)$ relation, and suggests that they be used for deducing the general set of parameters ρ, τ_f/τ, σ_b/σ_R, σ_R and δ_R.

With a firm understanding of the fragmentation process of single-fibre composites, it may now be feasible to examine and interpret the fibre breakage patterns in multi-fibre composites to gain some insight into the load transfer process. In principle, the knowledge of *in situ* fibre statistics and stress-recovery lengths allows one to assess the correlations between

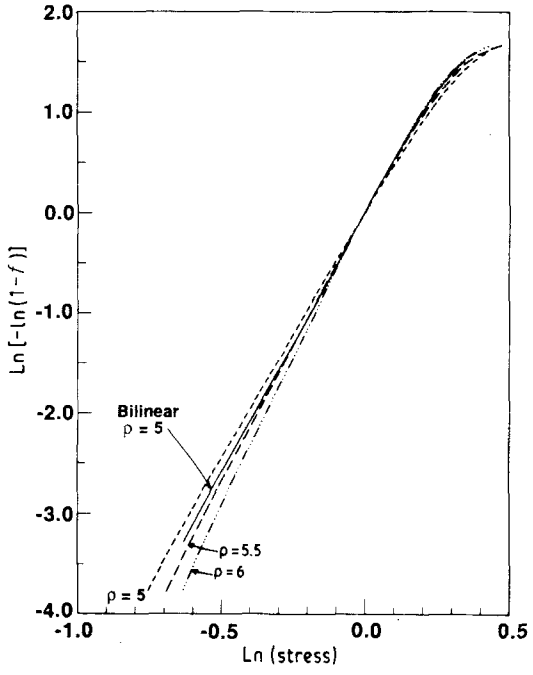

Figure 10 Weibull plot of fraction of breaks versus normalized stress for $\rho = 5$, $\tau_f/\tau = 0.3$, $\sigma_b/\sigma_R = 0.7$ and for linear recovery with $\rho = 5.0$, 5.5 and 6.0.

TABLE III Theory and simulation [3] results for mean number of fragments and mean fragment length versus σ_b/σ_R, τ_f/τ (bilinear recovery) at $\rho = 5$, nominal $L_T = 200$

σ_b/σ_R	τ_f/τ	L_T	N_T(sim)	N_T(theory)	$\bar{x}/\delta_R$(sim)	$\bar{x}/\delta_R$(theory)
0.5	0.3	196.8	59	57.8	3.336	3.413
0.6	0.3	197.6	63	63.2	3.147	3.130
0.7	0.3	197.3	69	69.3	2.868	2.855
0.8	0.3	198.6	77	76.8	2.573	2.592
0.9	0.3	198.2	83	84.3	2.377	2.355
1.0	0.3	198.1	97	92.1	2.033	2.156
0.7	0.3	197.3	69	69.3	2.868	2.855
0.7	0.5	198.6	90	86.2	2.217	2.308
0.7	0.7	198.3	100	98.0	1.983	2.025

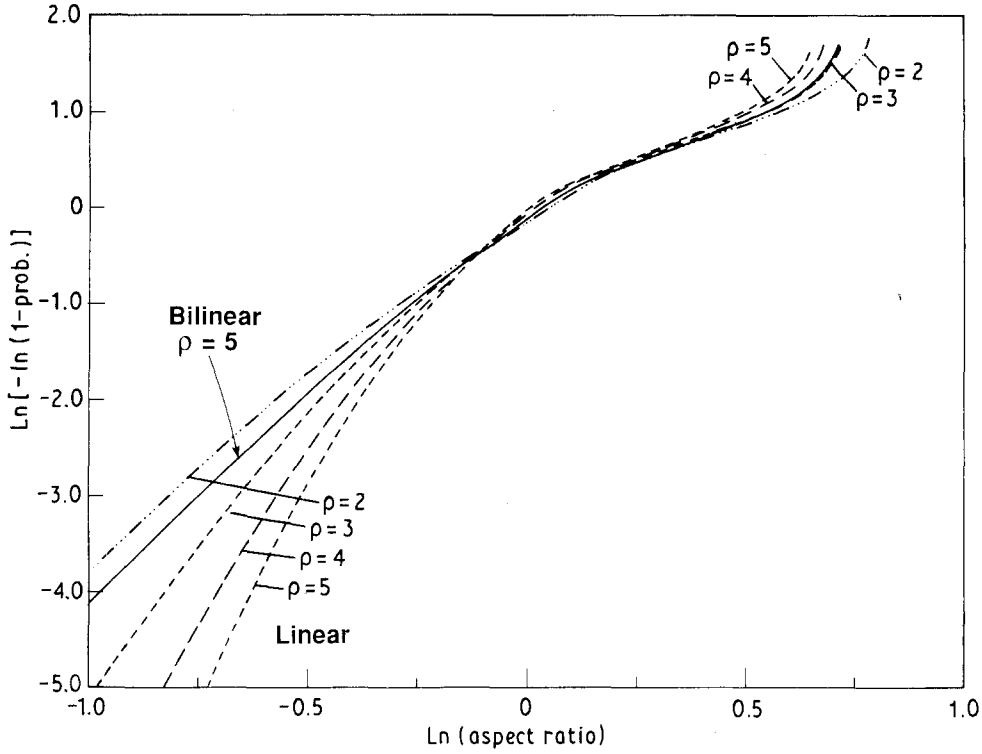

Figure 11 Final fragment distributions normalized to the mean fragment length for $\rho = 5$, $\tau_f/\tau = 0.3$, $\sigma_b/\sigma_R = 0.7$ and for linear recovery with $\rho = 2, 3, 4, 5$.

close breaks in neighbouring fibres. Such correlations arise because the load previously carried by a now-broken fibre is transferred on to the nearby fibres, leading to a non-uniform stress distribution in the neighbours and thus a higher probability of failure of the neighbours in the vicinity of the first failure. It is precisely the build up of such local correlated failures which leads to the ultimate failure of the entire composite once a critical number of fibres have failed in roughly the same plane. By observing the occurrence of nearby fibre breaks, one can, knowing the *in situ* fibre strength statistics at small lengths, work backwards to deduce how much load was transferred from one fibre on to another. Such information as obtained from actual experimental evaluation may prove invaluable.

The s.f.c. test is commonly applied to carbon fibre/epoxy matrix systems, but it may also be relevant for gaining information on metal-matrix composites (MMCs). Here, too, one has strong, stiff, brittle reinforcements embedded in a soft ductile matrix and the ultimate composite strength is controlled by the fracture of the reinforcements. The shear stress, τ, is usually assumed to be the plastic yield stress in shear, τ_y, of the matrix and this assumption, as well as changes in the reinforcement strength induced by processing, could easily be studied using s.f.c. tests. Although the matrix is not optically transparent in an MMC, the fibre fracture events can be monitored by acoustic emission (time-of-flight of acoustic pulses generated during fracture) as long as the fragment lengths are longer than the spatial resolution of this technique. The s.f.c. test thus holds the promise of yielding a wealth of much needed information on MMC materials.

Finally, the present theory is applicable to several other multiple-cracking problems which arise in composite materials. The first problem is that of the multiple matrix cracking which occurs in ceramic matrix composites reinforced with stiff fibres but with a sliding interface. In this case, the matrix exhibits cracking and the fibres transfer load to the matrix over a length δ associated with the sliding resistance τ. This problem is identical to the s.f.c. test here if one views the ceramic matrix as the multiple-cracking "fibre" and the reinforcing fibres as the elastic matrix medium containing this "fibre". The evolution of the matrix crack spacing with stress is then the same as that of the fragment distribution in the s.f.c. Hence, the present theory should allow for matrix cracking data to be inverted to obtain the interface and the failure statistics of the matrix material. The second problem is that of the multiple cracking of ceramic coatings on ductile substrates. This situation is the same as for an MMC except that the "fibre" is a thin film and the matrix exists only on one side of this film. Otherwise, the mechanics is largely identical and the present theory is useful for obtaining the coating/substrate shear strength and coating strength. Both of these problems have been studied using the unique-strength theory ($\rho \to \infty$) known previously, but the theory introduced here will allow for a better quantitative analysis of the fragmentation data.

In summary, we have discussed how fragmentation data from a single-filament composite test contains information on both *in situ* fibre strength and fibre matrix interfacial properties. To extract clearly such information from the data, we have developed an exact theory of the evolution of the fragment distribution with applied stress. The crux of the theory

involves continually removing (conceptually) the small fragments which cannot be further fragmented to leave only that portion of the fibre whose fragment distribution is exactly that of a unique-strength fibre with some appropriate break density. Because the fragment distribution of the unique-strength fibre problem is known exactly, the more general theory is also exact. The theory takes the form of a set of first-order differential equations describing the evolution of the removed fragments and the remaining fragmented fibre and, although non-linear, these equations are easily solved by iteration. We have demonstrated the success of the theory by showing the agreement between our predictions and "experimental" results obtained by computer simulations.

Acknowledgements

I thank Dr J. Kerins for pointing out Widom's exact solution to the sequential random addition problem, and Dr H. D. Wagner for introducing me to this fragmentation problem.

Appendix 1. Stress recovery including elastic shear stresses

In the main text, we discussed the fragmentation phenomenon in the context of a shear stress $\tau(x)$ which is independent of the applied stress. This condition certainly does not hold when only elastic stresses and strains are present in an elastic matrix with an elastic, well-bonded fibre. At low applied stresses, i.e. prior to any yielding or debonding, this is certainly the case and the shear stress is entirely elastic. And, even after yielding or debonding some of the stress recovery is still elastic in nature. In Appendix 1, we use the well known shear-lag analysis of Cox [11] to elucidate when elastic stresses are important and how to best account for them in our model.

Consider an elastic fibre of length l well-bonded to an elastic matrix under strain ε_0. The maximum stress which can be built up in the fibre is $\sigma_0 = E_{\text{fibre}}\varepsilon_0$. In the absence of any yielding or debonding at the interface, the stresses $\tau(x)$ at the interface and $\sigma(x)$ in the fibre are, within a shear-lag analysis [11]

$$\tau(x) = \alpha\sigma_0 \frac{\sinh[(\beta l/2)(1 - 2x/l)]}{\cosh(\beta l/2)} \quad \text{(A1a)}$$

and

$$\sigma(x) = \sigma_0\left\{1 - \frac{\cosh[(\beta l/2)(1 - 2x/l)]}{\cosh(\beta l/2)}\right\} \quad \text{(A1b)}$$

where α and β are constants given by Cox as

$$\alpha = [G_m/2E_f \ln(R/r)]^{1/2} \quad \text{(A2a)}$$

$$\beta = \frac{4}{d}\alpha \quad \text{(A2b)}$$

where G_m is the matrix shear modulus, d the fibre diameter, and r the fibre radius. The quantity R/r is related to the fibre fill fraction in Cox's treatment but R is better interpreted as the radial distance from the fibre axis at which the matrix strain is unaffected by the presence of the fibre [2]. For long fibres, $\beta \gg 1$, $\sigma(x) \simeq \sigma_0$ over most of the fibre length and $\tau(x) \simeq 0$ except near the fibre ends. $\tau(x)$ is a maximum at the fibre ends.

Clearly, $\sigma(x)$ never fully attains the value σ_0 for a finite length fibre, and thus the "recovery" length defined by Equation 3 is formally infinite. Moreover, as σ_0 is increased, the axial fibre stress is increased at all locations $0 < x < l$ in the fibre. Therefore, a stress exclusion zone where the stress remains at or below a constant value does not exist. This is evident in Fig. A1, which shows $\sigma(x)$ for three increasing values of applied stress. Supposing the break at $x = 0$ to have occurred at stress σ_1 in Fig. A1, we see that at higher stresses $\sigma > \sigma_1$ much of the fibre length also carries a load greater than σ_1. In particular, as σ increases, the region of fibre near the end with stress below σ_1 decreases steadily in length. Therefore, if only elastic stresses exist, the fibre fragmentation cannot be correctly described by our theory. We are currently working to establish a means for taking into account stress profiles such as those in Fig. A1a. Fortunately, many composite materials exhibit matrix yielding or interface debonding at stresses much lower than the typical fibre strengths. The stresses over which purely elastic behaviour prevails may then be small. In this case, few if any breaks will occur in the elastic regime and a linear approximation to the axial stress of $\sigma(x) = \beta\sigma_0 x$, $0 < x < \beta^{-1}$ and $\sigma(x) = \sigma_0$, $x > \beta^{-1}$, which corresponds to a stress-independent exclusion length $\delta = \beta^{-1}$, may be a reasonable approximation to the true stress profile of Equation A1b, as shown in Fig. A1. Once yielding or debonding begins, a true exclusion zone can be better defined, as we now show.

To investigate the influence of yielding/debonding imagine that as ε_0 (or σ_0) is increased $\tau(x = 0)$ reaches a critical value τ_f at which either (i) the interface fails in shear, or (ii) the matrix yields in shear. Then as σ_0 is increased further, a "debond" region forms at the fibre ends and propagates inward such that the shear stress

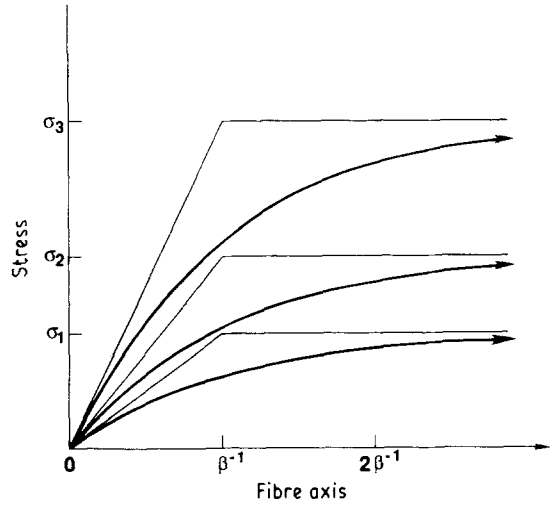

Figure A1 Axial stress profiles for purely elastic stresses. Note that as the applied stress increases, the stresses increase everywhere along the fibre length; hence no exclusion zone can rigorously be defined. An approximate exclusion zone of length β^{-1} independent of stress (lighter line) may be useful at low stresses, however.

at the tip of the debond remains at τ_f. In the debond region, the shear stress is given by some value τ_i (assumed constant in this discussion). In case (i) above, which may be most relevant for epoxy resin/carbon-fibre composites, τ_i is the frictional shear stress behind the debond. In case (ii) above, which is also relevant for metal-matrix composites, τ_i is the matrix yield stress τ_y and $\tau_i = \tau_y = \tau_f$ also.

The stresses in the fibre in the presence of the debond may now be determined. For an applied stress, σ_0, creating a debond of length d_b, the stresses behind the debond are

$$\tau(x) = \tau_i \qquad x \leq d_b \tag{A3a}$$

$$\sigma(x) = \frac{4\tau_i}{d}x \qquad x \leq d_b \tag{A3b}$$

For $x \geq d_b$, the elastic stresses still exist and are the same as the stresses in a fibre of length $l' = l - 2d_b$ under an "applied" stress $\sigma' = \sigma_0 - 4d_b\tau_i/d$, because an axial stress of $4d_b\tau_i/d$ is built up within the debond region. Thus, Equations A1a and b hold with $l' = l - 2d_b$, $\sigma' = \sigma_0 - 4d_b\tau_i/d$ and a new "fibre end" at $x = d_b$ so that with $x' = x - d_b$.

$$\tau(x) = \alpha\left(\sigma_0 - \frac{4d_b}{d}\tau_i\right)\frac{\sinh[(\beta l'/2)(1 - 2x'/l')]}{\cosh(\beta l'/2)} \qquad x > d_b \tag{A4a}$$

$$\sigma(x) = \frac{4d_b}{d}\tau_i + \left(\sigma_0 - \frac{4d_b}{d}\tau_i\right) \times\left[1 - \frac{\cosh[(\beta l'/2)(1 - 2x'/l')]}{\cosh(\beta l'/2)}\right] \qquad x > d_b \tag{A4b}$$

The debond length, d_b, is determined by requiring $\tau(x^+ = d_b) = \tau_f$, or using Equation A4a

$$\tau_f = \alpha\left(\sigma_0 - \frac{4d_b}{d}\tau_i\right)\tanh\left(\frac{\beta l'}{2}\right) \quad (l' = l - 2d_b) \tag{A5}$$

showing that d_b is determined by τ_f, σ_0 and τ_i, as expected. Equation A5 allows us to rewrite Equation A4a in the compact form

$$\tau(x) = \tau_f\frac{\sinh[(\beta l'/2)(1 - 2x'/l')]}{\sinh(\beta l'/2)} \qquad x \geq d_b \tag{A6}$$

which clearly exhibits the fixed value of τ_f at the debond tip. Finally, using equation A5 in Equation A4b allows us to express the axial stress recovery as

$$\sigma(x) = \frac{4\tau_i}{d}x \qquad x \leq d_b \tag{A6b}$$

$$\sigma(x) = \frac{4d_b}{d}\tau_i + \frac{\tau_f}{\alpha} \times\left[\frac{\cosh(\beta l'/2) - \cosh(\beta l'/2)(1 - 2x'/l')}{\sinh(\beta l'/2)}\right] \qquad x \geq d_b \tag{A6c}$$

which is one main result of this appendix.

The axial stress given above is shown schematically in Fig. A2. The important features to notice are the following. First, the total elastic stress is limited to τ_f/α because as the applied stress increases it is the debond length which grows, and the elastic recovery region is only translated along the fibre axis. If the typical fibre strengths are much larger than τ_f/α, then the stresses σ_0 during the s.f.c. test are typically $\sigma_0 \gg \tau_f/\alpha$ and thus most of the stress is taken up by the debond region. This, along with the fact that $\tau_i \leq \tau_f$, indicates that most of the stress recovery length is taken up by d_b also, i.e. $d_b \gg \beta^{-1}$ where β^{-1} is the length over which the elastic stress recovers exponentially. Second, the slope of $\sigma(x)$ at the debond tip is actually a constant, $d\sigma(x = d_b^+)/dx = 4\tau_f/d$, independent of both d_b and the applied stress, σ_0.

For this axial stress profile, a proper exclusion zone length, δ, can now be constructed. Recall that the important aspect of the exclusion zone is that within it, the stress never attains the value that it had before entering the exclusion zone. In this sense, all points within the exclusion zone have been "proof-tested" at a higher stress than they will experience during the remainder of the test; hence these points will not fail. We identify this length δ_0 at the applied stress σ_0, then, as the longest length δ_0 at which the stress at δ_0, $\sigma(\delta_0)$, will never exceed the current applied value σ_0, as the stress is increased further. At stress σ_0, corresponding to debond length d_b^0, we thus require δ_0 to satisfy

$$\sigma(\delta_0) \leq \sigma_0 = \frac{4d_b^0}{d}\tau_i + \tau_f/\alpha \tag{A7}$$

for all applied stress $\sigma > \sigma_0$, or equivalently all debond lengths $d_b > d_b^0$. Because within our theory the exclusion zone is associated with a single break, the length δ cannot itself depend on the fragment length l. Thus, we must neglect the effect of finite lengths l' in Equation A4b and take $l' \to \infty$ so our approximate

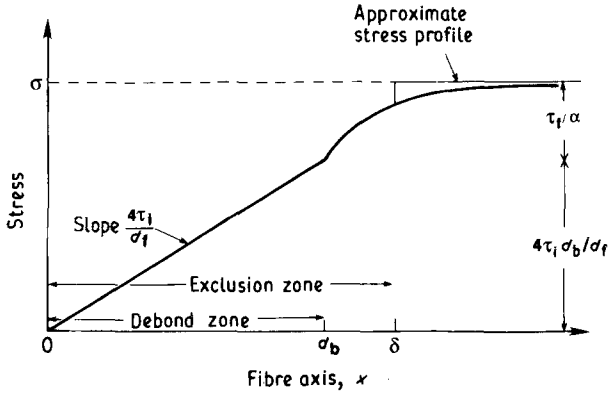

Figure A2 Axial stress profile including debonding/yielding and elastic stress recovery (bold line). Only a fixed fraction τ_f/α of the applied stress σ_0 is taken up by the elastic stress recovery. A rigorous exclusion zone δ_0 at stress σ_0 can be defined as (see Appendix 1)

$$\delta_0 = \frac{\sigma_0 d}{4\tau_i} - \frac{1}{\beta}\left[\frac{\tau_f}{\tau_i} - 1 + \ln\frac{\tau_i}{\tau_f}\right]$$

The approximate stress recovery profile needed to apply the present theory is shown as the lighter line.

stress at δ_0, $\sigma(\delta)$, is

$$\sigma(\delta_0) = \frac{4\tau_i}{d}\delta_0 \qquad \delta_0 < d_b \tag{A8a}$$

$$\sigma(\delta_0) = \frac{4d_b}{d}\tau_i + \tau_f/\alpha\,(1 - e^{-\beta(\delta_0 - d_b)}) \qquad \delta_0 > d_b \tag{A8b}$$

at the applied stresses, σ, corresponding to debond length d_b. Requiring Equation A7 to hold for all debonds, $d_b > d_0$ (i.e. all stresses greater than σ_0) is accomplished by taking the equality in Equation A7, $\sigma(\delta_0) = \sigma_0$, solving for δ_0 and minimizing with respect to the stress, or equivalently d_b. This yields an exclusion zone length

$$\delta_0 = d_b^0 + \frac{1}{\beta}[1 - \ln(\tau_i/\tau_f)] \tag{A9}$$

at stress σ_0 (debond length d_b^0). The exclusion zone length differs from the debond length by a length on the order of β^{-1}. For smaller τ_i, the exclusion zone length is larger. In terms of the applied stress σ_0, the exclusion zone length may be expressed, after some algebra, as

$$\delta_0 = \frac{\sigma_0 d}{4\tau_i} - \frac{1}{\beta}\left[\frac{\tau_f}{\tau_i} - 1 + \ln\left(\frac{\tau_i}{\tau_f}\right)\right]. \tag{A10}$$

In this form, δ_0 is similar to the linear stress recovery at constant τ_i but with a stress-independent correction. For the special case $\tau_i = \tau_f$ (matrix yielding at the interface), the correction term is precisely zero and $\delta_0 = \sigma_0 d/4\tau_i$, i.e. the exclusion zone length is the same as obtained if τ were a constant!

The exclusion length δ_0 given by Equation A10 is a rigorous lower bound even for finite length fragments in the sense that the stress within δ_0 of a break will never reach the value of σ_0. However, unlike the case shown in Fig. 2 where τ is a constant, the stress beyond the exclusion zone is still below the applied value $\sigma(x)$, $< \sigma_0$ for $x > \delta_0$. Therefore the assumption in the theory that the stress is a constant at the asymptotic value σ_0 for $x > \delta_0$ does not hold. The best approximation consistent with our theory is to model the stress recovery as shown in Fig. A2. δ_0 is given by Equation A10 but the stress beyond $x > \delta_0$ is approximated by σ_0. This approximation overestimates the stress near the end of the exclusion zone (within β^{-1}) and so overestimates the probability of failure in this region. The theory will thus predict slightly smaller fragment lengths. However, the magnitude of this error is fairly small: the maximum overestimate of the stress occurs for $\tau_f = \tau_i$ at $x = \delta_0$ and is only $0.37\,\tau_f/\alpha$. The length over which some overestimates exist is on the order of β^{-1}. The effects of this approximate stress profile are thus not significant when (i) the elastic stress recovery is small, $\tau_f/\alpha \ll \sigma_0$, and (ii) the typical fragment lengths are much longer than β^{-1}. The latter condition also ensures that the effects of overlap of stress recovery from the fibre ends, which lead to the hyperbolic rather than exponential behaviour in Equation A1, are also small. These conditions are usually satisfied in polymer and metal matrix materials. After using the present theory with the exclusion zone, Equation A10, these conditions can be checked experimentally to verify that application of the approximate exclusion zone is justified.

To summarize this appendix, we find that if only elastic stresses exist (no debonding or yielding) an exclusion zone cannot be property defined. However, once debonding/yielding has occurred at τ_f an approximate exclusion zone of length $\delta = d\sigma/4\tau_i - 1/\beta[\tau_f/\tau_i - 1 + \ln(\tau_i/\tau_f)]$, where τ_i is the shear stress behind the debond, can be defined and the stress profile in Fig. A2 is a good approximation if $\tau_f/\alpha \ll \sigma$ and if the fragment lengths are long compared to the elastic recovery length β^{-1}.

Appendix 2. Some formal restrictions on $\tau(x)$

In the text we considered a shear stress $\tau(x)$ which was independent of both σ_{app} and the recovery length δ. If $\tau(x)$ depends on δ via the form $\tau(x/\delta)$ then not all functional forms for such a $\tau(y)$ are consistent with the length δ being a true exclusion zone. Here we delineate the allowable forms of $\tau(y)$ such that δ is both the stress recovery length and the exclusion zone length. Recall that the exclusion zone at applied stress σ_0 is that region near the break where the stress is forevermore reduced below σ_0 even as the applied stress is increased indefinitely.

We suppose $\tau(x)$ to be of the form $\tau(x/\delta)$ where δ is the stress recovery length, i.e. $\sigma(\delta) = \sigma_{app}$. In this case, Equation 1 can be rewritten as

$$\sigma(x) = \frac{4\delta}{d}\int_0^{x/\delta} \tau(y)\,dy \qquad x \leq \delta \tag{A11}$$

and δ satisfies

$$\sigma(\delta) = \frac{4\delta}{d}\int_0^1 \tau(y)\,dy = \sigma_{app} \tag{A12}$$

or

$$\delta = \frac{d\sigma_{app}}{4\bar{\tau}}; \quad \bar{\tau} = \int_0^1 \tau(y)\,dy \tag{A13}$$

The recovery length δ_0 at applied stress σ_0 is also the exclusion zone length if $\sigma(x) < \sigma_0$ for all $x < \delta_0$ for all applied future stresses $\sigma_{app} > \sigma_0$. Using Equations A11–A13 this requirement can be expressed mathematically as

$$\sigma(x) = \sigma_{app}\frac{1}{\bar{\tau}}\int_0^{x/\delta} \tau(y)\,dy \leq \sigma_0 \qquad \text{for } x \leq \delta_0;\ \sigma_{app} \geq \sigma_0 \tag{A14}$$

where δ is the recovery length at stress σ_{app}. If Equation A14 is satisfied for $x = \delta_0$ then it is also satisfied for $x \leq \delta_0$. Equation A14 is then equivalent to

$$\sigma_{app}\frac{1}{\bar{\tau}}\int_0^{\delta_0/\delta} \tau(y)\,dy \leq \sigma_0 \qquad \sigma_{app} \geq \sigma_0 \tag{A15}$$

but because $\delta_0/\delta = \sigma_0/\sigma_{app}$, Equation A15 can be

rewritten as

$$\frac{1}{\bar{\tau}}\int_0^{\sigma_0/\sigma_{app}} \tau(y)dy \leq \sigma_0/\sigma_{app} \quad 0 \leq \sigma_0/\sigma_{app} \leq 1 \quad \text{(A16)}$$

Because Equation A16 must hold for all σ_0/σ_{app}, we use $x = \sigma_0/\sigma_{app}$ and write Equation A16 as

$$\frac{1}{\bar{\tau}}\int_0^x \tau(y)dy \leq x \qquad 0 \leq x \leq 1 \quad \text{(A17)}$$

This is the restriction on $\tau(y)$ if δ is the proper exclusion zone length. This restriction can be converted directly to a restriction on the shape of the axial stress recovery by using Equation 1 of the text and Equation A13

$$\frac{\sigma(x)}{\sigma_{app}} \leq x/\delta \qquad \text{for} \quad 0 < x < \delta \quad \text{(A18)}$$

This shows that the stress-recovery function must be below the linear line $\sigma(x) = \sigma_{app}\, x/\delta$.

An analysis similar in spirit to the present one can be used to determine the exact, or best approximate exclusion zone length for any $\tau(x)$ function, an example of which is given in Appendix 1. Note also that the bilinear stress recovery form utilized in the text satisfies the requirement of Equation A18.

Appendix 3. The unique-strength fragment distribution $P(x; n, \delta)$

The unique strength fragment distribution at density n and recovery length δ, $P(x; n, \delta)$, can be recast as the distribution of near-neighbour centre-to-centre distances of N hard rods of length δ thrown down randomly on a line of length L, but constrained not to overlap. Because the hard rods cannot penetrate, the minimum centre-to-centre separation is precisely δ and no rod can be inserted between two rods separated by less than 2δ. The statistics and distribution functions for equisized hard rods placed at fixed positions along a line has been solved elegantly by Widom, who called this process "sequential random addition" (s.r.a.)[4].

The desired distribution $P(x; n, \delta)$ is related to Widom's distribution of gaps $q(x; n\delta)$ in the s.r.a. problem by

$$P(x; n, \delta) = \frac{1}{n\delta^2}\, q(x; n\delta). \quad \text{(A19)}$$

The distribution q, in turn, is given by

$$q(x;\eta) = 2\int_0^\eta d\eta' \psi(\eta') e^{-(x/\delta - 1)\psi(\eta')} \qquad \delta \leq x \leq 2\delta \quad \text{(A20a)}$$

$$= \frac{\psi^2(\eta)}{\psi'(\eta)} e^{-(x/\delta - 2)\psi(\eta)} \qquad 2\delta \leq x \quad \text{(A20b)}$$

with $\eta = n\delta$ the dimensionless packing density and with the auxiliary function $\psi(\eta)$ defined implicitly by

$$\eta = \int_0^\psi \exp\left(-2\int_0^t \frac{1 - e^{-s}}{s} ds\right) dt \quad \text{(A21)}$$

The two functions required to solve the differential Equations 13 are particularly simple to relate to the function ψ

$$P(\delta; n, \delta) = \frac{q(\delta; n\delta)}{n\delta^2} = \frac{2}{\eta\delta}\int_0^\eta d\eta' \psi(\eta') \quad \text{(A22)}$$

and

$$\frac{L^*}{L} = \frac{N}{L}\int_{2\delta}^\infty dx(x - 2\delta) P(x; n, \delta) = \frac{1}{\psi'(\eta)} = \phi(\eta) \quad \text{(A23)}$$

Inverting Equation A21 to obtain $\psi(\eta)$ must be performed numerically but, with $\psi(\eta)$ in hand, all needed quantities associated with the sequential random addition problem, Equaions A19–A23, are easily obtained.

The analytical structure of $\psi(\eta)$ is of interest to evaluate. Note that as $n\delta$ approaches the maximum limit of $n\delta = \eta^*$, the available space for adding new breaks, L^*/L, goes to zero. Thus $\psi'(\eta^*) = \infty$ and, from Equation A20b, $\psi(\eta^*) = \infty$, and so from Equation A21

$$\eta^* = \int_0^\infty \left[e^{-2}\int_0^t \frac{1 - e^{-s}}{s} ds\right] dt = 0.7476\ldots \quad \text{(A24)}$$

reproducing the previously quoted mean fragment length $\bar{x}/\delta = 1/\eta^* = 1.337\ldots$. An asymptotic analysis of Equation A21 shows that [12]

$$\psi(\eta) = \frac{e^{-2\gamma}}{\eta^* - \eta} \qquad \eta \to \eta^* \quad \text{(A25)}$$

where $\gamma = 0.577\,216$ is Euler's constant. This form is accurate to four decimal places for $\eta \geq 0.70$ and is particularly useful for calculating the high density portions to Equations A22 and A23. The $(\eta^* - \eta)^{-1}$ divergence is typical of one-dimensional problems. Widom has also performed a low-density expansion of $\psi(\eta)$

$$\psi(\rho) = \eta + \eta^2 + \frac{7}{6}\eta^3 + \frac{13}{9}\eta^4 + \ldots \quad \text{(A26)}$$

and we have found that the approximate analytic form

$$\psi(\eta) = \frac{1}{(1 - \eta/\eta^*)^{\eta^*}} \quad \text{(A27)}$$

is accurate to within 1% for $\psi < 1$ ($\eta \leq 0.47$), although it does not exhibit the proper exponent of the $\eta \to \eta^*$ divergence. In any case, Equation A21 is not difficult to solve numerically and one can then create look-up tables for $P(\delta; n, \delta)$ and L^*/L, and $P(x; n, \delta)$ follows from Equations A19 and A20.

Appendix 4. Additional calculation details

Using Equations A19 and A23, the set of differential

equations for N, L and P_R becomes simply

$$\frac{dL}{d\sigma} = -\frac{L}{\delta} q(\delta; n\delta) \frac{d\delta}{d\sigma} \quad \text{(A28a)}$$

$$\frac{dN}{d\sigma} = -\frac{L}{\delta^2} q(\delta; n\delta) \frac{d\delta}{d\sigma} + \phi(n\delta) \frac{L}{L_0 \sigma_0} \rho(\sigma/\sigma_0)^{\rho-1} \quad \text{(A28b)}$$

and the "removed" distribution evolves according to

$$\frac{dP_R(x; \sigma)}{d\sigma} = \frac{L}{\delta^2} q(\delta; n\delta) \frac{d\delta}{d\sigma} \delta_D(x - \delta) \quad \text{(A29)}$$

These equations may be solved directly by numerically iterating. Interestingly, however, once nearly all the breaks have been added to the fibre the solutions for $\eta = N\delta/L$ only approach η^* very slowly. As σ, and hence δ, increases, a point is reached where $dN/d\sigma$ becomes negative, i.e. more fragments are removed than breaks added, and the product $N\delta/L$ then increases more slowly toward η^* as more and more fragments are removed from the "remaining" fibre. In fact, all the fragments can be removed by this procedure but it is not physically satisfying to have $N < 1$ and $L < 1$ but with $N\delta/L$ approaching η^*. It is thus convenient and physical to halt the iterating procedure when the probability of adding one more break anywhere in the remaining fibre drops below 1/2. This cut-off corresponds closely to cessation of the experimental test: no more breaks (less than 1/2 of a break) occur for arbitrarily large stress increases and so the fragment distribution is unchanged. The cut-off condition is thus

$$\frac{N}{\eta\delta} \int_{2\delta}^{\infty} dx\, q(x; \eta) = \frac{1}{2} \quad \text{(A30)}$$

because $1/\eta\, q(x; \eta)$ is the fraction of fragments of size x. Utilizing Equation A20b for $q(x)$ $x \geq 2\delta$ yields the condition

$$N\psi/\eta\psi' = \frac{N\psi\phi}{\eta} = \frac{1}{2} \quad \text{(A31)}$$

Because the cutoff nearly always occurs at high packing fractions $\eta \simeq \eta^*$ where the asymptotic form for ψ is accurate, $N\psi\phi/\eta = 1/2$ is nearly identical

$$\frac{N}{\eta}(\eta^* - \eta) = \frac{1}{2} \quad \text{(A32a)}$$

or

$$\eta = \left(\frac{\eta^*}{1 + 0.5/N}\right) \quad \text{(A32b)}$$

as the condition for determining the packing fraction η at which to halt the iteration process.

(a) Linear stress recovery

Here we further specialize to the situation where the shear stress is assumed constant, $\tau(x) = \tau$, so that the recovery length is linear with stress, $\delta = d\sigma/4\tau$. Before proceeding, it is useful to introduce length and stress scale parameters to non-dimensionalize the differential equations and make evident the basic input parameters. Let us rescale the stress by σ_R (to be specified below) and then all lengths by the recovery length $\delta_R = d\sigma_R/4\tau$ at the stress σ_R. Then rewriting Equations A28a and b using the dimensionless variables

$$s = \sigma/\sigma_R \quad \text{(A33a)}$$

$$h = \delta/\delta_R \quad \text{(A33b)}$$

$$L = L/\delta_R;\ L_T = L_T/\delta_R;\ L_0 = L_0/\delta_R \quad \text{(A33c)}$$

(we leave it understood that all fibre lengths L are now in units of δ_R) we obtain, noting that now also $h = s$

$$\frac{dL}{ds} = -\frac{L}{s} q(\delta; \eta) \quad \text{(A34a)}$$

and

$$\frac{dN}{ds} = -\frac{L}{s^2} q(\delta; \eta) + L\phi(\eta) \rho s^{\rho-1} \frac{\rho}{L_0} (\sigma_R/\sigma_0)^{\rho} \quad \text{(A34b)}$$

One convenient choice for σ_R is then clearly that which reduces $1/L_0(\sigma_R/\sigma_0)^{\rho}$ to unity. Because $L_0 = L_0/\delta_R = L_0/(d\sigma_R/4\tau)$, this leads to

$$\sigma_R = \left(\frac{4\tau}{d} L_0 \sigma_0^{\rho}\right)^{1/(\rho+1)} \quad \text{(A35)}$$

which is related by a factor of $2^{1/(\rho+1)}$ to the scaling parameter selected by Henstenburg and Phoenix and used by us in the main text [3]. The set of equations in this reduced form depends only on the input parameters, ρ, and the non-dimensional initial fibre length, $L_T = L_T/\delta_R$. One must keep in mind, however, that the underlying scale parameters σ_R and δ_R themselves depend on σ_0, L_0, ρ and τ, which are the quantities we ultimately wish to derive from experimental distributions.

References

1. R. GULINO and S. L. PHOENIX, *J. Mater. Sci.*, in press.
2. A. N. NETRAVALI, R. B. HENSTENBURG, S. L. PHOENIX and D. SCHWARTZ, *Polym. Compos.* **10** (1989) 226.
3. R. B. HENSTENBURG and S. L. PHOENIX, *ibid.* **10** (1989).
4. B. WIDOM, *J. Chem. Phys.* **44** (1966) 3888.
5. A. KELLY and W. R. TYSON, *J. Mech. Phys. Solids* **13** (1965) 329.
6. A. C. KIMBER and J. G. KEER, *J. Mater. Sci. Lett.* **1** (1982) 353.
7. W. A. FRASER, F. H. ANCKER, A. T. DiBENEDETTO and B. ELBIRLI, *Polym. Compos.* **4** (1983) 238.
8. L. T. DRZAL, M. J. RICH and P. F. LLOYD, *J. Adhesion* **16** (1982) 1.
9. L. T. DRZAL, M. J. RICH, M. F. KOENIG and P. F. LLOYD, *ibid.* **16** (1983) 133.
10. S. H. OWN, R. V. SUBRAMANIAN and S. C. SAUNDERS, *J. Mater. Sci.* **21** (1986) 3912.
11. A. KELLY and N. H. MacMILLAN, "Strong Solids", 3rd Edn (Clarendon Press, Oxford, 1986) Ch. 6.
12. H. SCHER, private communication.

Received 8 October
and accepted 19 November 1990